Generalized needle solutions, interfacial instabilities, and pattern formation

Jian-Jun Xu
Department of Mathematics and Statistics, McGill University, Montreal, Quebec, Canada H3A 2K6
(Received 22 March 1995; revised manuscript received 16 November 1995)

During the past several years, the study of interfacial instability and pattern formation phenomena has preoccupied many researchers in the broad area of nonlinear science. These phenomena occur in a variety of dynamical systems, far from equilibrium, especially in some practically very important physical systems, always displaying some fascinating patterns at the interface between solid and liquid or liquid and another liquid. A prototype of these phenomena is dendrite growth in solidification. It is now well recognized that this phenomenon is induced by some global interfacial instabilities involved in the systems. In the present article, we shall consider the generalized needle crystal solution and its stability properties. In terms of the unified asymptotic approach developed in the previous papers, two different types of global instability mechanisms have been identified: (1) the global trapped wave instability, and (2) the instability caused by perturbations with zero frequency that we call the null-f instability. It connects the so-called microscopic solvability condition theory. On the basis of these results, a solution to the selection problem for pattern formation is clarified. [S1063-651X(96)01605-4]

PACS number(s): 68.70.+w, 81.10.Fq, 81.10.Mx

I. INTRODUCTION

Dendritic growth is a common interfacial phenomenon in phase transition and crystal growth. In the past several decades, this important subject has preoccupied a large number of investigators in the broad areas of condensed matter physics, materials science, applied mathematics, fluid dynamics, etc. (e.g., [1–34]).

The first important result in dendrite growth was Ivantsov's zero surface tension, steady needle crystal solution published in 1947 ([1]). But the Ivantsov solution did not solve the problem of dendrite growth. Specifically, being a similarity solution, the Ivantsov solution cannot predict the growth rate of the needle tip. The second important contribution to this subject was made by Schaefer, Glicksman, and Ayers, who identified the selection problem. Schaefer, Glicksman, and Ayers performed a series of careful experiments on dendrite growth, and measured the tip velocities under various conditions, by using transparent organic material succinonitrile (SCN), and correctly concluded that at the later stage of dendrite growth, the dendrite's tip velocity is a uniquely determined function of the growth condition and the material properties (see [4,5]). From then on, a great effort has been made to resolve this selection problem. The basic problems have been (i) what is the mechanism which determines tip growth velocity and (ii) what is the origin and essence of dendritic structure formation? These problems are of great significance in industrial application as well as theoretical research. To solve these problems, understanding of the role played by the surface tension for the instability mechanisms involved in the system is crucial. For steady dendrite growth with the inclusion of nonzero surface tension, Nash and Glicksman gave a well-known mathematical formulation with two parameters: the undercooling parameter T_∞ and the isotropic surface tension parameter ε (see [3]). Nash and Glicksman assumed that as the boundary conditions the dendrite had a smooth tip and infinitely long root approaching the Ivantsov solution in the far field. The Nash-Glicksman problem has been extensively studied by a large number of investigators, and the far field condition imposed by Nash and Glicksman has been adopted by most authors without objection. It was discovered during the 1980s by a number of researchers that the Nash-Glicksman problem has no solution (see [11–13]). Only with the inclusion of another parameter, the anisotropy of surface tension α_4, may the classic needle solutions for the Nash-Glicksman problem exist. These results led to the so-called microscopic solvability condition theory, which has influenced the scientific community on a large scale for about a decade ([9,10]).

Despite the fact that the classic needle solution does not exist for the Nash-Glicksman problem without anisotropy of surface tension, the system may allow a nonclassic, nearly steady, or ''slightly'' time evolving, needle solution with a smooth stem, which is very long, say, of $O(1/\varepsilon)$, but finite. Evidently, such nonclassic needle solutions are physically acceptable. Thus the essential issue is the stability of these nonclassic needle solutions and its connection with pattern formation and selection of dendrite growth.

It is well understood now that the isotropic surface tension may induce oscillatory instability, the so-called global trapped wave (GTW) mechanism. However, the questions about the role of the anisotropy of surface tension for dendrite growth, whether the anisotropy may invoke a new instability mechanism or not, and if it does, what the implication of this new instability for the pattern formation and selection is, are still not fully answered.

In the present paper we intend, by using the two-dimensional dendrite growth problem as a framework, to attack these problems.

In terms of the unified asymptotic method developed in our previous work, we found that a dendrite growth system with anisotropic surface tension is subject to two different types of instability mechanisms.

(1) ''The global trapped wave instability'' mechanism, which is induced by perturbations with high frequency. This mechanism was discovered by Xu in 1991 analytically (see

 © 1996 The American Physical Society

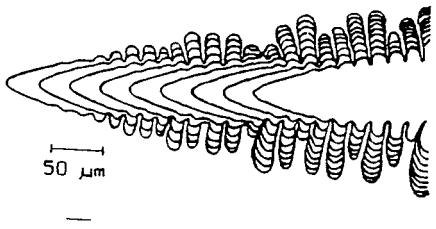

FIG. 1. Typical dendrite growth from a supersaturated solution.

[25]) for a dendrite with sole isotropic surface tension. It is only slightly affected by anisotropy.

(2) The so-called ''zero-frequency instability'' (null-f) mechanism, which is induced by perturbations with zero frequency. This is a new mechanism generated only by the anisotropy and has a close connection with the microscopic solvability condition (MSC) theory of steady needle crystal growth.

Based on these findings, we are able to draw the following scenario. When the anisotropy parameter is larger than a critical number, the system is dominated by the null-f instability mechanism. Hence the selected dendrite growth solution may be the steady needle crystal solution that was first predicted by MSC theory. However, when the anisotropy parameter is smaller than this critical number, the system will be dominated by the GTW instability mechanism. Hence the selected dendrite growth solution in this range can never be the steady needle solution. Instead, it will be the GTW neutral mode. When the anisotropy of surface tension tends to zero, the null-f instability mechanism disappears, while the GTW instability mechanism remains. These conclusions are in good agreement with experimental observations and numerical simulations.

The present paper is arranged as follows. In Sec. II we briefly describe the mathematical formulation for the problem of two-dimensional dendrite growth from a pure melt. In Sec. III we give a linear perturbed system for perturbations around the generalized needle solution. In Sec. IV we give the outer solution. In Sec. V we give the inner solution in the vicinity of a singular point. In Sec. VI we derive the GTW mechanism and null-f mechanism. In Sec. VII we give the selection conditions and discussions.

II. MATHEMATICAL FORMULATION OF TWO-DIMENSIONAL DENDRITE GROWTH FROM A PURE MELT

We study the problem of two-dimensional free dendrite growth from a pure substance. The reasons for doing so have two aspects. First, this model is practical. Two-dimensional dendrite growth can be obtained in a Hele-Shaw cell. Secondly, the mathematical treatment for the two-dimensional model is relatively simpler than that for a three-dimensional model, and the instability mechanisms for both cases are similar.

A typical two-dimensional dendrite growth is shown in Fig. 1. We assume that a free dendrite is growing with a tip velocity $U(t)$ into an undercooled pure melt with the undercooling temperature $T_\infty < T_{M0}$, where T_{M0} is the melting temperature of a flat interface. The thermal length $l_T = \kappa_T/U$ is used as the length scale, where the characteristic velocity U may be a typical value or the average value of the tip velocity $U(t)$. The quantity $\Delta H/c_p$ is used as the temperature scale. Here, κ_T is the thermal diffusivity, while ΔH is the latent heat release per volume of solid phase. We adopt the parabolic cylindrical coordinate system (ξ,η) moving with the characteristic velocity U defined as follows:

$$x/\eta_0^2 = \tfrac{1}{2}(\xi^2 - \eta^2), \quad y/\eta_0^2 = \xi\eta, \tag{2.1}$$

where η_0^2 is a constant to be determined by locating the tip of the steadily growing dendrite on the parabola $\eta = 1$. It will be seen later that this constant is the Peclet number for the case of zero surface tension. The unknown functions for the present problem are the temperature fields in the liquid and solid phases, $T(\xi,\eta,t)$, $T_S(\xi,\eta,t)$, and the interface shape $\eta_s(\xi,t)$. The nondimensional governing equation for the problem is simply the heat conduction equation. The boundary conditions include the upstream far field condition, the Gibbs-Thomson condition, and the heat balance condition on the interface. The coefficient of surface tension, γ, may have anisotropy. The commonly acceptable form of γ is

$$\gamma = \hat{\gamma} A_s(\theta), \qquad A_s(\theta) = 1 - \alpha_m \cos(m\theta), \tag{2.2}$$

where $\hat{\gamma}$ is the isotropic surface tension coefficient, α_m is the anisotropy coefficient, and θ is the orientation angle. Typically, for the fourfold anisotropy, one can set the integer $m = 4$. As a result,

$$A_s(\theta) = f(\xi)/(1+\xi^2)^2, \qquad f(\xi) = (1-\alpha_4)(1+\xi^2)^2 + 8\alpha_4\xi^2. \tag{2.3}$$

Thus the system involves three nondimensional parameters: the undercooling temperature $T_\infty < 0$, the isotropic surface tension parameter $\varepsilon = \sqrt{l_c/l_T}/\eta_0^2 = \sqrt{l_c U/\kappa}/\eta_0^2$, and anisotropy parameter α_4. Here, l_c is the capillary length defined as

$$l_c = \frac{\hat{\gamma} c_p T_{M0}}{(\Delta H)^2}. \tag{2.4}$$

III. BASIC STATE SOLUTION AND UNSTEADY PERTURBED SYSTEM

It is well known that for zero surface tension ($\varepsilon = 0$) and arbitrary undercooling, the system allows the following similarity solution (see [1]):

$$T = T_*(\eta) = T_\infty + \eta_0^2 e^{\eta_0^2/2} \int_\eta^\infty e^{-\eta_0^2\eta_1^2/2} d\eta_1, \qquad T_S = T_{S*} = T_*(1) = 0, \qquad \eta_* = 1, \tag{3.1}$$

$$T_\infty = -\eta_0^2 e^{\eta_0^2/2}\int_1^\infty e^{-\eta_0^2\eta_1^2/2} d\eta_1,$$

$$(0 \leqslant \xi < \infty),$$

where the constant η_0^2 is uniquely determined as a function of the undercooling T_∞. The radius of curvature of the parabolic interface $\eta_*=1$ at the tip $\xi=0$ is $l_b=\eta_0^2 l_T$ and η_0^2 is actually the Peclet number, namely, $\mathrm{Pe}=\eta_0^2$.

During the past decade, there has been a long argument for the existence of a steady state solution for the case of $\varepsilon \neq 0$. The key is how to formulate the steady problem. We point out that although the system indeed does not allow a classic steady needle solution for the case of isotropic surface tension, it always has some slightly time dependent solutions describing the later stage of pattern evolution.

These solutions may depend on a slow time variable, defined as $\overline{t}=\varepsilon(t-t_0)$, where $t_0 \gg 1$. We assume that the total lengths of dendrite in these solutions are very long, but finite, which may be increasing with time, such as $L(\varepsilon)=(\overline{t}+C)/\varepsilon$ $[C=O(1)]$; furthermore, at the root the solutions are close to the Ivantsov parabola, namely,

$$\{T, T_s, \eta_s\} = \{T_*, T_{S*}, \eta_*\} + O(\varepsilon) \quad [\text{as } \xi = L(\varepsilon)]. \tag{3.2}$$

It can be proved that for any fixed $\overline{t}>0$, as $\varepsilon \to 0$ these solutions, $q_B=:\{T, T_s, \eta_s\}$, all have the same steady regular perturbation expansion:

$$q_B(\xi, \eta, \overline{t}, \varepsilon) \sim q_* + \varepsilon^2 q_1 + \varepsilon^4 q_2 + \cdots, \tag{3.3}$$

with the Ivantsov solution $q_*=:\{T_*, T_{S*}, \eta_*\}$ as the leading term. These solutions may contain some time-dependent terms, but these terms are all exponentially small in the region away from the root. Thus these solutions may be physically considered as the steady solutions. We call the above broad class of slightly time-dependent solutions the nearly steady state solution, or the generalized steady needle solutions.

In this paper we shall not look into the exact form of such generalized steady needle solutions, which will be studied elsewhere. Instead, we shall use these generalized steady needle solutions as the basic states, and attempt to study their stability property. We point out that the exact form of these basic states is not important. For our purpose, the only information that we need is that these solutions exist and in the region away from the root, they can be well approximated by the steady Ivantsov solution, i.e.,

$$T_B(\xi, \eta, \varepsilon) = T_*(\eta) + O(\varepsilon^2),$$

$$T_{SB}(\xi, \eta, \varepsilon) = O(\varepsilon^2), \tag{3.4}$$

$$\eta_B(\xi, \varepsilon) = 1 + O(\varepsilon^2).$$

We consider perturbations around these basic states and separate the general unsteady solutions into two parts:

$$T = T_B + \tilde{T}(\xi, \eta, t, \varepsilon),$$

$$T_S = T_{SB} + \tilde{T}_S(\xi, \eta, t, \varepsilon), \tag{3.5}$$

$$\eta_s = \eta_B + \tilde{h}(\xi, t, \varepsilon)/\eta_0^2,$$

in which the perturbations, $\tilde{q}=:\{\tilde{T}; \tilde{T}_S; \tilde{h}\}$, are assumed to be generated by initial infinitesimal disturbances with a characteristic amplitude $\tilde{\delta} \ll 1$. Hence a linearization in $\tilde{\delta}$ is applicable. The linearized perturbed system is a homogeneous system shown below:

$$\left(\frac{\partial^2}{\partial \xi^2} + \frac{\partial^2}{\partial \eta^2}\right)\tilde{T} - \eta_0^4(\xi^2+\eta^2)\frac{\partial \tilde{T}}{\partial t} + \eta_0^2\left(\xi\frac{\partial \tilde{T}}{\partial \xi} - \eta\frac{\partial \tilde{T}}{\partial \eta}\right) = 0,$$

$$[0 \leqslant \xi \leqslant L(\varepsilon)], \tag{3.6}$$

with the following boundary conditions.

$$(1)\text{As} \quad \eta \to \infty, \quad \tilde{T} \to 0; \tag{3.7}$$

$$(2)\text{As} \quad \eta \to 0, \quad \tilde{T}_S = O(1). \tag{3.8}$$

(3) The interface conditions: making the Taylor expansions around the interface of the generalized needle crystal, it follows that at $\eta=\eta_B(\xi,\varepsilon)$

$$\tilde{T} - \tilde{T}_S = \left\{\frac{\partial T_B}{\partial \eta} - \frac{\partial T_{SB}}{\partial \eta}\right\}\tilde{h}/\eta_0^2, \tag{3.9}$$

$$\tilde{T}_S = \frac{\varepsilon^2 A_s(\xi)}{\hat{S}(\xi)}\left\{\frac{\partial^2 \tilde{h}}{\partial \xi^2} + \frac{\xi}{\hat{S}^2(\xi)}\frac{\partial \tilde{h}}{\partial \xi} - \frac{1}{\hat{S}^2(\xi)}\tilde{h}\right\}, \tag{3.10}$$

$$\frac{\partial}{\partial \eta}(\tilde{T} - \tilde{T}_S) + \eta_0^2 \hat{S}^2(\xi)\frac{\partial \tilde{h}}{\partial t} + \xi\frac{\partial \tilde{h}}{\partial \xi} + \tilde{h} + \left\{\frac{\partial^2}{\partial \eta^2}[T_B - T_{SB}]\right\}\frac{\tilde{h}}{\eta_0^2}\left\{\frac{\partial^2}{\partial \xi^2}[T_B - T_{SB}]\right\}\frac{\tilde{h}'}{\eta_0^2} = 0, \tag{3.11}$$

where

$$\hat{S}(\xi) = \sqrt{\xi^2 + \eta_B^2}. \tag{3.12}$$

(4) The root condition: at $\xi=L(\varepsilon)$,

$$\{\tilde{T}, \tilde{T}_s, \tilde{h}\}(L) = 0. \tag{3.13}$$

(5) The tip smoothness condition: at $\xi=0$,

$$\frac{\partial}{\partial \xi}\{\tilde{T}; \tilde{T}_S; \tilde{h}\} = 0$$

for the symmetrical modes (S modes), (3.14)

$$\{\tilde{T}; \tilde{T}_S; \tilde{h}\} = 0$$

for the antisymmetrical modes (A modes). (3.15)

System (3.6)–(3.15) leads to a linear eigenvalue problem, when one considers the type of solutions, $\tilde{q}=\hat{q}e^{\sigma t}$. The ei-

genvalue σ will be a function of the parameters ε, α_4, and η_0^2. We shall solve this eigenvalue problem by using matched asymptotic methods.

IV. MULTIPLE VARIABLE EXPANSION SOLUTIONS IN THE OUTER REGION

We first look for the asymptotic expansion for solutions $\tilde{q}(\xi,\eta,t,\varepsilon)$ of the linear system (3.6)–(3.15) in the limit $\varepsilon\to 0$, in terms of the multiple variable expansion (MVE) method. In doing so, we introduce a set of fast variables $\{\xi_+,\eta_+,t_+\}$:

$$\xi_+=\frac{\xi}{\varepsilon},\quad \eta_+=\frac{\eta-1}{\varepsilon},\quad t_+=\frac{t}{\varepsilon}, \tag{4.1}$$

and define the stretched variables $(\xi_{++},\eta_{++},t_{++})$ as

$$\xi_{++}=\int k(\xi,\varepsilon)d\xi_+,\quad \eta_{++}=g(\xi,\varepsilon)\eta_+,\quad t_{++}=t_+/\eta_0^2. \tag{4.2}$$

In terms of these variables, we make the following multiple variable expansion for the perturbed state:

$$\begin{aligned}\tilde{T}&=\{\tilde{T}_0(\xi,\eta,\xi_{++},\eta_{++})+\varepsilon\tilde{T}_1(\xi,\eta,\xi_{++},\eta_{++})\\&\quad+\cdots\}e^{\sigma t_{++}},\\ \tilde{h}&=\{\tilde{h}_0(\xi,\xi_{++})+\varepsilon\tilde{h}_1(\xi,\xi_{++})+\cdots\}e^{\sigma t_{++}},\\ k&=k_0+\varepsilon k_1+\varepsilon^2k_2+\cdots,\\ g&=k_0+\varepsilon g_1+\varepsilon^2g_2+\cdots,\\ \sigma&=\sigma_0+\varepsilon\sigma_1+\varepsilon^2\sigma_2+\cdots,\end{aligned} \tag{4.3}$$

where $\sigma=\sigma_R-i\omega$; $(\omega\geqslant 0)$ is the eigenvalue and the fast variables and slow variables $(\xi,\eta,\xi_{++},\eta_{++},t_{++})$ in the eigenfunction solution are treated formally as independent variables. One can convert the above linear perturbed system into a system with the multiple variables $(\xi,\eta,\xi_{++},\eta_{++},t_{++})$ as shown in [22], and successively derive each order approximation in the outer region $[0\leqslant\xi<L(\varepsilon)]$. For the zeroth-order approximation, we derive

$$\left(\frac{\partial^2}{\partial\xi_{++}^2}+\frac{\partial^2}{\partial\eta_{++}^2}\right)\tilde{T}_0=0,\quad \left(\frac{\partial^2}{\partial\xi_{++}^2}+\frac{\partial^2}{\partial\eta_{++}^2}\right)\tilde{T}_{S0}=0, \tag{4.4}$$

and the following boundary conditions.

$$(1)\ \text{As}\ \ \eta_{++}\to\infty,\ \ \tilde{T}_0\to 0, \tag{4.5}$$

$$(2)\ \text{As}\ \ \eta_{++}\to-\infty,\ \ \tilde{T}_{S0}\to 0, \tag{4.6}$$

(3) on the interface, at $\eta_{++}=0,\ \eta=1$

$$\tilde{T}_0=\tilde{T}_{S0}+\tilde{h}_0, \tag{4.7}$$

$$\tilde{T}_{S0}=\frac{A_s(\xi)k_0^2}{S(\xi)}\frac{\partial^2\tilde{h}_0}{\partial\xi_{++}^2}, \tag{4.8}$$

$$k_0\frac{\partial}{\partial\eta_{++}}(\tilde{T}_0-\tilde{T}_{S0})+\sigma_0S^2(\xi)\tilde{h}_0+k_0\xi\frac{\partial\tilde{h}_0}{\partial\xi_{++}}=0, \tag{4.9}$$

where $S(\xi)=\sqrt{1+\xi^2}$.

(4) The root condition: as $\xi\to\infty$, one should have

$$\{\tilde{T}_0;\tilde{T}_{S0};\tilde{h}_0\}=0. \tag{4.10}$$

(5) The tip smoothness condition: at $\xi=0$,

$$\text{(i)}\ \ \frac{\partial}{\partial\xi}\{\tilde{T}_0;\tilde{T}_{S0};\tilde{h}_0\}=0\quad\text{for the } S \text{ modes,} \tag{4.11}$$

$$\text{(ii)}\ \ \{\tilde{T}_0;\tilde{T}_{S0};\tilde{h}_0\}=0\quad\text{for the } A \text{ modes.} \tag{4.12}$$

The system (4.4)–(4.12) has the following normal mode solutions:

$$\begin{aligned}\tilde{T}_0&=A_0(\xi,\eta)\exp\{i\xi_{++}-\eta_{++}\},\\ \tilde{T}_{S0}&=B_0(\xi,\eta)\exp\{i\xi_{++}+\eta_{++}\},\\ \tilde{h}_0&=\hat{D}_0\exp\{i\xi_{++}\}.\end{aligned} \tag{4.13}$$

The coefficient $\hat{D}_0$ in the zeroth-order approximation is set as a constant.

From (4.7)–(4.9), we derive that the wave number function $k_0(\xi)$ must be subject to the local dispersion formula

$$\sigma_0=\Sigma(\xi,k_0)=\frac{k_0}{S^2}\left[1-\frac{2A_s(\xi)k_0^2}{S}\right]-i\frac{\xi k_0}{S^2}. \tag{4.14}$$

For any fixed eigenvalue σ_0, one can solve three wave numbers as the functions of ξ, namely, $\{k_0^{(1)}(\xi),k_0^{(2)}(\xi),k_0^{(3)}(\xi)\}$, with $(\mathrm{Re}\{k_0^{(1)}\}>\mathrm{Re}\{k_0^{(3)}\}>0>\mathrm{Re}\{k_0^{(2)}\})$. Thus, for a fixed σ_0, the system allows three fundamental wave solutions $\{H_1,H_2,H_3\}$, corresponding to the wave number functions $k_0^{(1)},k_0^{(2)},k_0^{(3)}$, respectively. The solution H_1 is called the short wave branch, while the solution H_3 is called the long wave branch. The solution H_2, having a negative wave number $(\mathrm{Re}\{k_0^{(2)}\}<0)$, is ruled out. Its corresponding perturbed temperature field $\tilde{T}$ will grow exponentially as $\eta\to\infty$, violating the boundary condition (4.5). Thus the general solution of the zeroth-order approximation is

$$\begin{aligned}\tilde{h}_0&=D_1H_1(\xi)+D_3H_3(\xi)\\&=D_1\exp\left\{\frac{i}{\varepsilon}\int_0^\xi k_0^{(1)}d\xi_1\right\}+D_3\exp\left\{\frac{i}{\varepsilon}\int_0^\xi k_0^{(3)}d\xi_1\right\}.\end{aligned} \tag{4.15}$$

Here, the coefficients $\{D_1,D_3\}$ are arbitrary constants to be determined.

It has been noted that the MVE solution (4.3) has a singular point ξ_c in the complex ξ plane, which is the root of the equation

$$\frac{\partial\Sigma(k_0,\xi)}{\partial k_0}=6A_sk_0^2-(1-i\xi)S=0, \tag{4.16a}$$

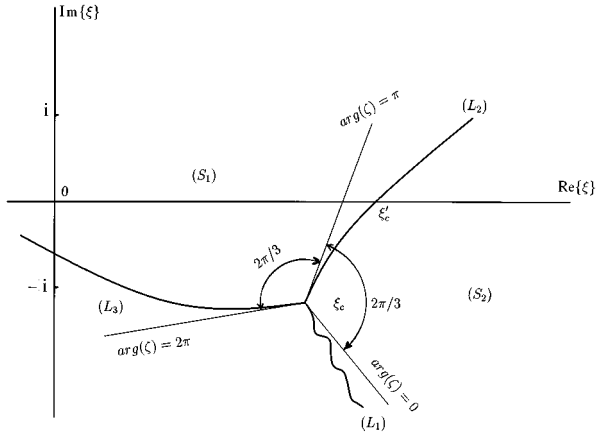

FIG. 2. The sketch of Stokes line (L_1), (L_2) emanating from the turning point ξ_c, in the case of complex spectrum $|\sigma|=O(1)$.

or

$$\sigma_0=e^{-i3\pi/4}\left(\frac{2}{27}\right)^{1/2}\frac{(\xi+i)^{7/4}(\xi-i)^{1/4}}{\sqrt{f(\xi)}}. \qquad (4.16b)$$

Due to the existence of this singularity, the MVE solution (4.3) is not uniformly valid in the whole complex ξ plane. In particular, the coefficients $\{D_1,D_3\}$ may be different constants in different sectors. These sectors are divided by the Stokes lines emanating from the singular point ξ_c. This is the so-called Stokes phenomenon. The so-called Stokes line is defined as

$$\mathrm{Im}\left\{\int_{\xi_c}^{\xi}(k_0^{(1)}-k_0^{(3)})d\xi'\right\}=0. \qquad (4.17)$$

The sketch of these Stokes curves $(L_1),(L_2),(L_3)$ for a typical case is shown in Fig. 2. The Stokes curve (L_2) divides the whole complex ξ plane into the sectors (S_1) and (S_2). We denote the coefficients of the solution (4.15) by $\{D_1,D_3\}$ in (S_1), and by $\{D_1',D_3'\}$ in (S_2). In order to determine the connection formula of these constants in different sectors, in order to obtain the uniformly valid asymptotic solution, one must divide the whole complex ξ plane into two regions: the inner region near the turning point ξ_c, and the outer region away from ξ_c. The solution (4.15) is only the outer solution valid in the outer region. One also needs to find the inner solution in the inner region, and match the inner solution with the outer solution.

Note that as $\xi\to\infty$, the solution H_1 increases exponentially, whereas H_3 decreases exponentially. Thus it follows that to satisfy the root condition (4.10), one must set the coefficient $D_1'=0$. Hence the root condition can be replaced by the following radiation condition that we imposed in previous work:

$$\widetilde{h}_0\sim D_3'H_3 \quad (\text{as } \xi\to\infty). \qquad (4.18)$$

Hereby, the constant D_3' is proportional to the characteristic amplitude of the initial perturbation $\widetilde{\delta}$. It is a free parameter in the linear theory. The remaining problem now is how to determine the coefficients D_1,D_3 in the MVE solution (4.15) in sector (S_1). In the next section, we shall study the inner solution near the singular point ξ_c. Then, the connection condition between the coefficients $\{D_1,D_3\}$ in sector (S_2) and $\{D_1'=0;D_3'=D'\}$ in sector (S_1) will be derived.

V. THE INNER SOLUTIONS NEAR THE SINGULAR POINT ξ_c

As indicated before, at ξ_c in the complex ξ plane, the MVE solution has a singularity. However, the true solution, after analytical continuation, should be regular at this point. Therefore the solution must have a different asymptotic form in the vicinity of ξ_c. In the inner region, $|\xi-\xi_c|\ll 1$; $|\eta-1|\ll 1$, we introduce the inner variables

$$\xi_*=\frac{\xi-\xi_c}{\varepsilon^{\alpha}}, \quad \eta_*=\frac{\eta-1}{\varepsilon^{\alpha}}, \qquad (5.1)$$

where α is to be determined. Besides, we denote the interface shape function as

$$\eta_s(\xi,t)=1+\frac{\widetilde{h}}{\eta_0^2}=1+\varepsilon^{\alpha}\eta_{*s}, \quad \eta_{*s}=\frac{\hat{h}(\xi_*,t)}{\eta_0^2}, \qquad (5.2)$$

so we have

$$\widetilde{h}(\xi,t)=\varepsilon^{\alpha}\hat{h}(\xi_*,t). \qquad (5.3)$$

Denote also

$$\widetilde{T}(\xi,\eta,t)=\varepsilon^{\alpha}\hat{T}(\xi_*,\eta_*,t),$$
$$\widetilde{T}(\xi,\eta,t)_S=\varepsilon^{\alpha}\hat{T}_S(\xi_*,\eta_*,t). \qquad (5.4)$$

We look for the mode solutions and make the inner expansions

$$\hat{T}(\xi_*,\eta_*,t)=\{\nu_0(\varepsilon)\widetilde{T}_0(\xi_*,\eta_*)+\nu_1(\varepsilon)\hat{T}_1(\xi_*,\eta_*)+\cdots\}e^{\sigma t/\varepsilon\eta_0^2},$$
$$\hat{T}_S(\xi_*,\eta_*,t)=\{\nu_0(\varepsilon)\widetilde{T}_{S0}(\xi_*,\eta_*)+\nu_1(\varepsilon)\hat{T}_{S1}(\xi_*,\eta_*)+\cdots\}e^{\sigma t/\varepsilon\eta_0^2},$$
$$\hat{h}=\{\nu_0(\varepsilon)\hat{h}_0+\nu_1(\varepsilon)\hat{h}_1+\cdots\}e^{\sigma t/\varepsilon\eta_0^2}. \qquad (5.5)$$

In terms of the inner variables, perturbed system (3.6)–(3.11) can be expressed in the form

$$\left(\frac{\partial^2}{\partial\xi_*^2}+\frac{\partial^2}{\partial\eta_*^2}\right)\hat{T}=\left\{\varepsilon^{2\alpha-1}\sigma\eta_0^2(\xi^2+\eta^2)-\varepsilon^{\alpha}\eta_0^2\left(\xi\frac{\partial}{\partial\xi_*}-\eta\frac{\partial}{\partial\eta_*}\right)-\varepsilon^{\alpha}\left(\frac{1}{\xi}\frac{\partial}{\partial\xi_*}+\frac{1}{\eta}\frac{\alpha}{\partial\eta_*}\right)\right\}\hat{T}, \qquad (5.6)$$

with the following boundary conditions.

$$(1)\ \text{As}\ \ \eta_*\to\infty,\ \ \hat{T}\to 0. \tag{5.7}$$

$$(2)\ \text{As}\ \ \eta_*\to-\infty,\ \ \hat{T}_S\to 0. \tag{5.8}$$

(3) At the interface, $\eta_*=0$,

$$\hat{T}=\hat{T}_S+\hat{h}+(\text{higher-order terms}), \tag{5.9}$$

$$\hat{T}_S=\frac{\varepsilon^{2-2\alpha}A_s(\xi)}{S(\xi)}\frac{\partial^2\hat{h}}{\partial\hat{\xi}_+^2}+(\text{higher-order terms}), \tag{5.10}$$

$$\varepsilon^{1-\alpha}\frac{\partial}{\partial\eta_*}(\hat{T}-\hat{T}_S)+\sigma S^2(\xi)\hat{h}+\varepsilon^{1-\alpha}\xi\frac{\partial\hat{h}}{\partial\xi_*}=(\text{higher-order terms}). \tag{5.11}$$

Letting $\varepsilon\to 0$, under the condition

$$\varepsilon^{2\alpha-1}\sigma_0\ll 1, \tag{5.12}$$

the above inner system can be further simplified into the following third-order ordinary differential equation for the interface perturbation $\hat{h}$:

$$i\frac{2\varepsilon^{3-3\alpha}A_s(\xi)}{S}\frac{\partial^3\hat{h}}{\partial\xi_*^3}+\varepsilon^{1-\alpha}(\xi+i)\frac{\partial\hat{h}}{\partial\xi_*}+\sigma_0S^2\hat{h}=O(\text{higher-order terms}). \tag{5.13}$$

For further discussion, we transform the outer solution $\tilde{h}$ into a new unknown function $W(\xi)$, by using the transformation introduced in [22]:

$$\tilde{h}=W(\xi)\exp\left\{\frac{i}{\varepsilon}\int_{\xi_c}^{\xi}k_c(\xi_1)d\xi_1\right\} \tag{5.14}$$

and accordingly, in the inner region, we set

$$\hat{h}=\hat{W}(\xi_*)\exp\left\{\frac{i}{\varepsilon}\int_{\xi_c}^{\xi}k_c(\xi_1)d\xi_1\right\}. \tag{5.15}$$

Letting

$$\left(\frac{\partial S^2\Sigma}{\partial k_0}\right)_{k_0=k_c}=\frac{6A_sk_c^2}{S}+(1-i\xi)=0 \tag{5.16}$$

or

$$k_c(\xi)=\left(\frac{S}{6A_s}(1-i\xi)\right)^{1/2}=e^{-i\pi/4}(\xi+i)^{7/4}(\xi-i)^{5/4}/\sqrt{6f(\xi)}\qquad(\mathrm{Re}\{k_c\}>0), \tag{5.17}$$

Eq. (5.13) can be transformed to

$$\varepsilon^{3-3\alpha}\Omega_3\frac{d^3\hat{W}}{d\xi_*^3}+i\varepsilon^{2-2\alpha}\Omega_2\frac{d^2\hat{W}}{d\xi_*^2}+iS^2[\sigma_0-\Sigma_c(\xi)]\hat{W}=O(\text{higher-order terms}), \tag{5.18}$$

where

$$\Omega_3=-\frac{2A_s(\xi)}{S},$$

$$\Omega_2=-\frac{6k_cA_s(\xi)}{S}=-e^{-i\pi/4}\frac{6^{1/2}f^{1/2}}{S^2}\left(\frac{\xi+i}{\xi-i}\right), \tag{5.19}$$

$$\Sigma(k_c,\xi)=\Sigma_c(\xi)=e^{-i3\pi/4}\left(\frac{2}{27}\right)^{1/2}\frac{(\xi+i)^{7/4}(\xi-i)^{1/4}}{\sqrt{f(\xi)}}.$$

Clearly, at the singular point ξ_c,

$$\sigma_0-\Sigma_c(\xi_c)=0. \tag{5.20}$$

Hence the singular point ξ_c is actually a turning point of the inner equation (5.18). The variable ξ in the coefficient functions of Eq. (5.18) also needs to be changed to the inner variable ξ_* by $\xi=\xi_c+\varepsilon^{\alpha}\xi_*$. Next, we need to make Taylor expansions around ξ_c for the coefficient functions and balance the leading terms on the left hand side of Eq. (5.18), in the limit $\varepsilon\to 0$, to determine the value of α. Note that

$$f(\xi)=(1-\alpha_4)(\xi^2+a_1^2)(\xi^2+a_2^2), \tag{5.21}$$

where

$$a_1\approx 1-\sqrt{2\alpha_4},\quad a_2\approx 1+\sqrt{2\alpha_4}\quad(\text{as}\ \ \alpha_4\ll 1). \tag{5.22}$$

The function $f(\xi)$ has four imaginary zeros $(\pm ia_1,\pm ia_2)$. Hence, in addition to ξ_c, the inner equation has two more turning points: $\xi=\pm i$, and four other singular points: $\xi=(\pm ia_1;\pm ia_2)$. The relative positions of these singular points to ξ_c are related to the values of the parameters σ_0, α_4. We choose the turning point ξ_c with $\mathrm{Re}\{\xi_c\}>0$; $\mathrm{Im}\{\xi_c\}<0$. So, the singular points $\xi=(i;ia_1;ia_2)$ are always away from ξ_c. Their influence on the inner solution is negligible. However, as $\sigma_0\to 0$, $\xi_c\to -i$, while as $\alpha_4\to 0$, $(-ia_1;-ia_2)\to -i$. So, the singular points $\xi=-i$, $-ia_1$, and $-ia_2$ may enter into the inner region of ξ_c and consequently influence the behavior of the inner solution under some circumstances. Two cases are found to be significant. (I) $\sigma_0=O(1)$: all the singular points $\xi=\pm i$ and $\xi=\pm ia_i$ $(i=1,2)$ are away from ξ_c; (II) $|\sigma_0|\ll 1$ and the singular points $\xi=-i$ and $\xi=-ia_i$ $(i=1,2)$ are inside the inner region. For these two cases, the inner equation in the far field of the inner region, as $\xi_*\gg 1$, can be reduced into the common form

$$\frac{d^2\hat{W}_0}{d\hat{\xi}_*^2}+\hat{\xi}_*^{p_0}\hat{W}_0=0, \tag{5.23}$$

where

$$\hat{\xi}_*=\frac{B}{\varepsilon^{\alpha}}(\xi-\xi_c), \tag{5.24}$$

and the constants B, p_0, and the scale number α are different for different cases. Moreover, for both cases, the Stokes line (L_2) that is tangential to the direction $\arg(\zeta)=\pi$ at the turning point ξ_c always intersects the real axis of ρ at a point ξ_c'

>0, and divides the real axis into two parts, respectively, in the sectors (S_1) and (S_2) (see Fig. 2). The general solution of Eq. (5.23) is

$$\hat{W}_0 = D_1 \hat{\xi}_*^{1/2} H_\nu^{(1)}(\zeta) + D_2 \hat{\xi}_*^{1/2} H_\nu^{(2)}(\zeta) \quad (\zeta = 2\nu \hat{\xi}_*^{1/2\nu}), \tag{5.25}$$

where $\nu = 1/(p_0+2)$ and $H_\nu^{(1)}(\zeta)$ and $H_\nu^{(2)}(\zeta)$ are the first and second kinds of Hankel functions of order ν, respectively. The above described results are summarized: For case (I): $\sigma_0 = O(1)$; $\alpha = \frac{2}{3}$, $p_0 = 1$, and $\nu = \frac{1}{3}$; for case (II): $|\sigma_0| = O(\varepsilon^{3/7})$, $\alpha_4 = O(\varepsilon^{8/7})$; $\alpha = \frac{4}{7}$, $p_0 = \frac{7}{4}$, and $\nu = \frac{4}{15}$.

We now turn to matching the inner solution (5.25) with the outer solution (4.15) in the intermediate regions in each sector. From the Hankel function theory, we have the connection formula: as $\pi < \arg(\zeta_1) < 2\pi$,

$$H_\nu^{(2)}(\zeta_1) = H_\nu^{(2)}(\zeta e^{i\pi}) = 2\cos(\nu\pi) H_\nu^{(2)}(\zeta) + e^{i\nu\pi} H_{1/3}^{(1)}(\zeta) \quad [0 \leqslant \arg(\zeta) \leqslant \pi] \tag{5.26}$$

and the following asymptotic forms: as $|\zeta| \to \infty$,

$$H_\nu^{(1)}(\zeta) \sim \left(\frac{2}{\pi\zeta}\right)^{1/2} e^{i\zeta - i(\nu/2 + 1/4)\pi} \quad [-\pi < \arg(\zeta) \leqslant 2\pi],$$
$$H_\nu^{(2)}(\zeta) \sim \left(\frac{2}{\pi\zeta}\right)^{1/2} e^{-i\zeta + i(\nu/2 + 1/4)\pi} \quad [-2\pi < \arg(\zeta) \leqslant \pi]. \tag{5.27}$$

By using these formulas, we first match the inner solution (5.25) with the outer solution (4.15) as $\hat{\xi}_* \to \infty$ in the sector (S_2). Note that in this sector, the outer solution, satisfying the radiation condition (4.18), has $D_1' = 0$. Thus, to match with the outer solution, one must set $D_1 = 0$ and $D_2 = D = D_3' \times \text{const} \neq 0$ in (5.25).

Furthermore, in terms of (5.26)–(5.27), we derive that in order to match the inner solution with the outer solution in the sector (S_1), the parameter σ_0 must be such a function of ε that, as $\varepsilon \to 0$,

$$\left(\frac{D_1}{D_3}\right) \exp\left\{\frac{i}{\varepsilon}\int_0^{\xi_c} [k_0^{(1)} - k_0^{(3)}] d\xi\right\} = i2\cos(\nu\pi). \tag{5.28}$$

So far, we have not applied the tip condition. Once the tip condition (4.11) or (4.12) is applied, the eigenvalue σ_0, as the function ε and α_4, can be determined by the condition (5.28). We find that the system allows two different types of spectra of eigenvalues: (1) The complex eigenvalues, $\sigma_0 = (\sigma_R - i\omega)$; $\omega > 0$, with $|\sigma_0| = O(1)$; and (2) the real eigenvalues with $|\sigma_0| \ll 1$. As a consequence, the system is subject to two different types of instability mechanisms: the global trapped wave instability, induced by perturbations with a high frequency, $|\omega| = O(1)$ and the low-frequency (null-f) instability mechanism, induced by perturbations with low frequency, $\omega = 0$. In the next section, we shall derive these results.

VI. THE SPECTRA OF EIGENVALUES AND INSTABILITY MECHANISMS

A. The global trapped wave instability

Consider $\sigma_0 = \sigma_R - i\omega$ and $\omega > 0$. With the complex eigenvalue σ_0, the physical solution in the outer region is

$$\mathrm{Re}\{(\tilde{h}_0(\xi,t)\} = \mathrm{Re}\{D_1 H_1 + D_3 H_3) e^{\sigma_0 t/\varepsilon \eta_0^2}\}. \tag{6.1}$$

To satisfy the tip smooth conditions, the coefficients D_1, D_3 must be subject to the following conditions: (i) for the symmetrical S modes,

$$D_3/D_1 = -k_0^{(1)}(0)/k_0^{(3)}(0), \tag{6.2}$$

(ii) for the antisymmetrical A modes,

$$D_1 = -D_3. \tag{6.3}$$

Combining (5.28) with (6.2), or (6.3), one obtains the following quantization conditions:

$$\chi = \frac{1}{\varepsilon}\int_0^{\xi_c} (k_0^{(1)} - k_0^{(3)}) d\xi = (2n + 1 + \tfrac{1}{2} + \theta_0)\pi - i\{\ln\ \alpha_0 + \ln[2\cos(\nu\pi)]\},$$
$$\alpha_0 e^{i\theta_0\pi} = k_0^{(1)}(0)/k_0^{(3)}(0) \quad \text{for the } S \text{ modes},$$
$$\alpha_0 = 1, \quad \theta_0 = 0 \quad \text{for the } A \text{ modes},$$
$$n = (0, \pm 1, \pm 2, \pm 3, \ldots). \tag{6.4}$$

It can be proved that the system only allows the complex eigenvalues with $|\sigma_0| = O(1)$, corresponding to the case (I) discussed in the last section. Consequently, one has $\nu = \frac{1}{3}$. This complex spectrum contains two discrete sets of complex eigenvalues for S modes and A modes, respectively, given by the quantization conditions (6.4) as

$$\sigma_0^{(n)}, \ (n = 0, \pm 1, \pm 2, \ldots) \sim (\varepsilon, \alpha_4).$$

It is found that these GTW mode solutions are slightly varying functions of the anisotropy parameter α_4, and the A-modes are more stable than the corresponding neutral S-modes.

In Fig. 3 we show, in the complex σ plane, the eigenvalues for the A-modes with various ε for given $n = 0,1,2$, $\alpha_4 = 0$. It is very interesting to see that these eigenvalues for $n = 0,1,2,\ldots$ appear to be located on the same curve in the complex σ plane, and direct to the point $\sigma = (\sigma)_{\max} = 0.2712$ as $\varepsilon \to 0$.

The system allows a unique neutrally stable n mode $(\sigma_R = 0)$, as $\varepsilon = \varepsilon_{*n}$, where $\varepsilon_{*0} = \varepsilon_* > \varepsilon_{*1} > \varepsilon_{*2} > \cdots$. In Fig. 4(a) we show the variation of ε_* with α_4, while Fig. 4(b) shows ω_* versus α_4.

B. The low-frequency (null-f) instability

We now turn to deriving the spectrum of real eigenvalues σ_0. In this case, the physical solution in the outer region becomes

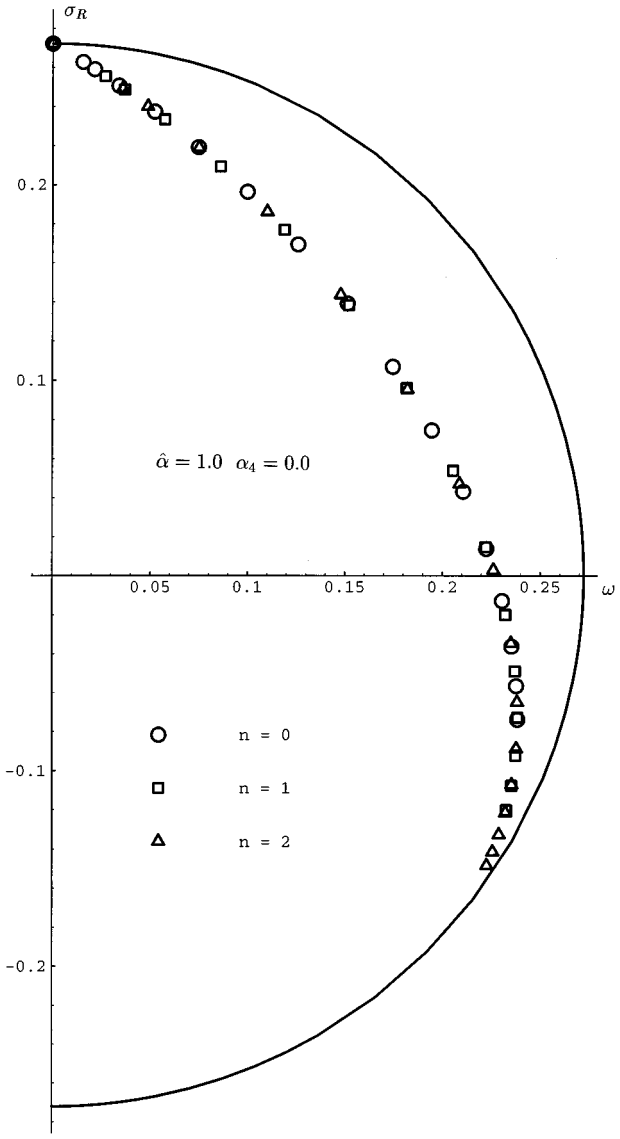

FIG. 3. The variations of $\sigma=\sigma_R-i\omega$ of GTW, A modes ($n=0,1,2$) in the complex σ plane with ε for the case $\alpha_4=0$ and $\hat{\alpha}=1$, where the parameter $\hat{\alpha}=\kappa_{TS}/\kappa_T$ is the ratio of the thermal diffusivities in solid and liquid phases.

$$\mathrm{Re}\{\tilde{h}_0(\xi,t)\}=R(\xi)e^{\sigma_0 t/\varepsilon}\eta_0^2, \tag{6.5}$$

$$R(\xi)=\mathrm{Re}\{D_1H_1+D_3H_3\}.$$

Note that as $\xi\ll 1$, $k_0^{(i)}(\xi)=k_0^{(i)}(0)+i2a_i\xi+O(\xi^2)$ $(i=1,3)$, where $k_0^{(i)}$ and a_i are real. Hence we can write

$$R(\xi)=[D_{1R}\cos(\chi_1)-D_{1I}\sin(\chi_1)]e^{-a_1\xi^2/\varepsilon} +[D_{3R}\cos(\chi_3)-D_{3I}\sin(\chi_3)]e^{-a_3\xi^2/\varepsilon}+O(\xi^3), \tag{6.6}$$

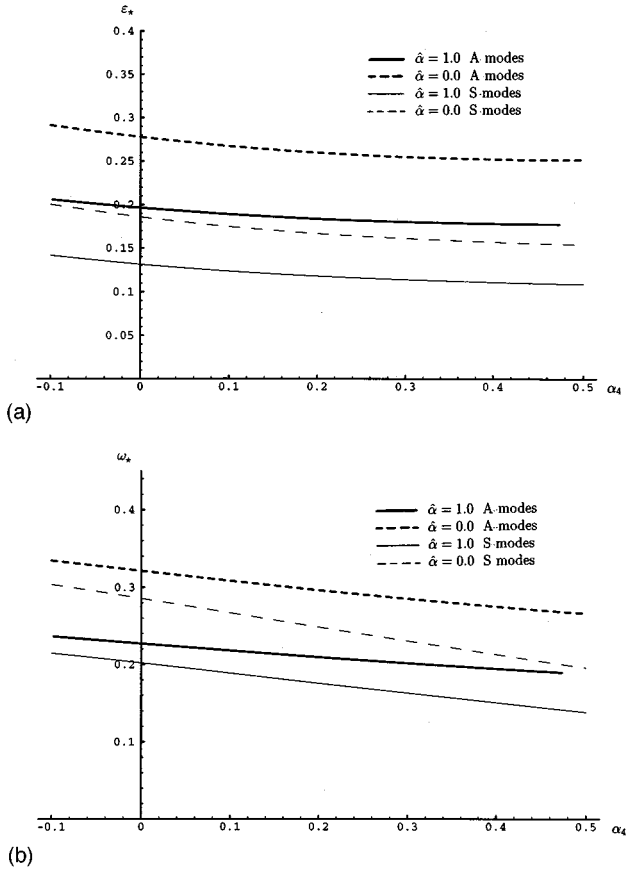

FIG. 4. (a) The variations of critical numbers ε_* corresponding to the neutrally stable GTW A mode and S modes versus α_4. (b) The variations of frequency of oscillations ω_* of neutrally stable GTW A mode and S modes versus α_4. (The solid lines are for the symmetric model, $\hat{\alpha}=1$, while the dashed lines are for one-sided model $\hat{\alpha}=0$.)

$$R'(\xi)=-[D_{1R}\sin(\chi_1)+D_{1I}\cos(\chi_1)]\frac{k_0^{(1)}(0)}{\varepsilon}e^{-a_1\xi^2/\varepsilon} -[D_{3R}\sin(\chi_3)+D_{3I}\cos(\chi_3)]\frac{k_0^{(3)}(0)}{\varepsilon}e^{-a_3\xi^2/\varepsilon} +O(\xi), \tag{6.7}$$

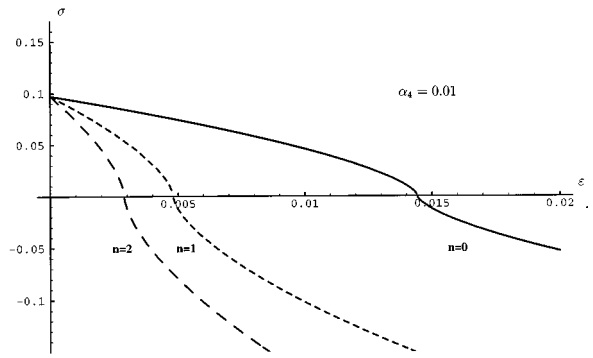

FIG. 5. The real eigenvalues σ $(n=0,1,2)$ of null-f mechanism versus ε for the case $\hat{\alpha}=1$, $\alpha_4=0.01$.

where

$$\chi_i=\frac{\xi}{\varepsilon}\,k_0^{(i)}(0)\quad (i=1,3). \tag{6.8}$$

Without losing generality, we can assume D_1 is a positive real number and denote

$$D_1>0,\quad D_3=|D_3|e^{i\chi_0\pi}. \tag{6.9}$$

Therefore the tip condition for the symmetric modes, $R'(0)=0$, leads to the condition $D_{3I}=0$, or

$$\frac{D_1}{D_3}=\left|\frac{D_1}{D_3}\right|e^{-i\chi_0\pi}\quad (\chi_0=0,1). \tag{6.10}$$

Furthermore, for the antisymmetric modes the tip condition, $R(0)=0$, leads to

$$\left|\frac{D_1}{D_3}\right|=-\cos(\chi_0\pi)\leqslant 1. \tag{6.11}$$

Combining (5.28) with the tip conditions (6.10) or (6.11), we obtain that

$$\mathrm{Re}\{\chi\}=(2n+\tfrac{1}{2}+\chi_0)\pi\quad (n=0,\pm 1,\pm 2,\ldots), \tag{6.12}$$

$$\left|\frac{D_1}{D_3}\right|=2\cos(\nu\pi)e^{\mathrm{Im}\{\chi\}}, \tag{6.13}$$

where

$$\chi_0=\begin{cases}0\ \text{ or }\ 1 & \text{for } S \text{ modes}\\ 1+\dfrac{\cos^{-1}|D_1/D_3|}{\pi} & \text{for } A \text{ modes.}\end{cases} \tag{6.14}$$

The quantization condition (6.12) determines the eigenvalues $\sigma_0^{(n)}$, while the formula (6.13) determines the corresponding eigenfunction. We did not find the real eigenvalues with $|\sigma_0|=O(1)$ from (6.12). But the system does allow a real spectrum with $|\sigma_0|\ll 1$. To derive it, we can first simplify the quantization condition (6.12) with the assumption $|\sigma_0|\ll 1$. In fact, from the local dispersion formula (4.14) one can derive that

$$[k_0^{(1)}-k_0^{(3)}]=\frac{1}{\sqrt{2}}\frac{(1-i\xi)^{7/4}(1+i\xi)^{5/4}}{f^{1/2}(\xi)}-\frac{3}{2}(1+i\xi)\sigma_0+O(\sigma_0^2). \tag{6.15}$$

We compute that

$$\begin{aligned}\chi&=\frac{1}{\varepsilon}\int_0^{\xi_c}(k_0^{(1)}-k_0^{(3)})d\xi\\&=\left(\int_0^{-ia_1}\right)+\left(\int_{-ia_1}^{-i}\right)+\left(\int_{-i}^{\xi_c}\right)\\&=\frac{1}{\varepsilon}\left\{\frac{i}{\sqrt{2}}\mathscr{R}-\frac{1}{\sqrt{2}}\gamma_0+i\,\frac{9}{4}\sigma_0+3(\sqrt{3}-1)\sigma_0(\xi_c+i)\right.\\&\quad\left.+O(\text{higher-order terms})\right\},\end{aligned} \tag{6.16}$$

where

$$\gamma_0=C_0\alpha_4^{7/8},\quad C_0\approx 1.802\,05,\quad \mathscr{R}\approx 0.615\,622. \tag{6.17}$$

Thus we obtain

$$\mathrm{Re}\{\chi\}=\frac{1}{\varepsilon}\left\{-\frac{\gamma_0}{\sqrt{2}}+C_1\sigma_0^{11/7}\alpha_4^{2/7}\right\}, \tag{6.18}$$

$$\mathrm{Im}\{\chi\}=\frac{1}{\varepsilon}\left\{\frac{\mathscr{R}}{\sqrt{2}}+\frac{9}{4}\sigma_0+C_2\sigma_0^{11/7}\alpha_4^{2/7}\right\}, \tag{6.19}$$

where

$$\begin{aligned}C_1&=3(\sqrt{3}-1)2^{3/7}3^{6/7}\cos(5\pi/14)\approx 3.2886,\\C_2&=3(\sqrt{3}-1)2^{3/7}3^{6/7}\sin(5\pi/14)\approx 6.2883.\end{aligned} \tag{6.20}$$

Having substituted these results in (6.12), it is shown that one must have $\alpha_4^{7/8}=O(\varepsilon)$ and $\sigma_0^{11/7}\alpha_4^{2/7}=O(\varepsilon)$. This relationship of the orders of magnitude between α_4, σ_0, and ε is just consistent with the case (II) discussed in the preceding section. Hence we have $\nu=\frac{4}{15}$. Moreover, it is also shown that the system does not allow any growing A mode for the null-f mechanism; only growing S modes are permissible. The quantization condition for these S modes is obtained as follows:

$$C_1\sigma_0^{11/7}\alpha_4^{2/7}=\frac{C_0}{\sqrt{2}}\alpha_4^{7/8}-\varepsilon(n+\tfrac{1}{2})\pi, \tag{6.21}$$

$$\left|\frac{D_1}{D_3}\right|=2\cos(4\pi/15)e^{\mathrm{Im}\{\chi\}}, \tag{6.22}$$

where

$$\mathrm{sgn}\left\{\frac{D_1}{D_3}\right\}=\begin{cases}1, & n=\text{even integer}\\-1, & n=\text{odd integer.}\end{cases} \tag{6.23}$$

For any fixed ε and α_4, from the quantization condition (6.21), one can solve a discrete set of the eigenvalue $\{\sigma_n\}$ $(n=0,1,2,3,\ldots)$ as shown in Fig. 5. It is seen that there is a discrete set of neutral stable modes ($\sigma_n=0$), corresponding to $\varepsilon_0'>\varepsilon_1'>\varepsilon_2'>\cdots>\varepsilon_n'>\cdots$. These neutral modes coincide with the steady needle crystal growth solutions predicted by MSC theory. For the neutral mode $n=0$, we obtain

$$\varepsilon=\varepsilon_a=\varepsilon_0'=\mathscr{K}\alpha_4^{7/8}, \tag{6.24}$$

where $\mathscr{K}=0.811\,20$. This coefficient, suggested by the MSC theory for the steady needle solutions with the largest tip velocity ($n=0$), has a different value, $\mathscr{K}=1.09$.

A remark should be made here that, as one can see from (4.3), the exact eigenvalue σ has the asymptotic expansion

$$\sigma=\sigma_0+\varepsilon\sigma_1+\varepsilon^2\sigma_2+\cdots\quad (\text{as } \varepsilon\to 0). \tag{6.25}$$

So far, we only calculated its leading-order approximation, σ_0. For the neutral modes of the null-f mechanism, when we set $\sigma_0=0$, the effect of σ_1 becomes important. Hence the critical numbers ε_n' for the neutral modes obtained above

will be inaccurate. For more accurate values of these critical numbers, one needs to include higher-order terms. For instance, one should solve ε_n' from the equation $\sigma_0+\varepsilon\sigma_1=0$.

There are $(m+1)$ purely growing modes and infinitely many decaying modes, as $\varepsilon_{m+1}<\varepsilon<\varepsilon_m$. As $\varepsilon\to 0$, the first n eigenvalues σ_k $(k=0,1,2,\ldots,n)$ all tend to the upper limit $\sigma'_{\max}$, which can be calculated as

$$\sigma'_{\max}=\alpha_4^{3/8}\left[\frac{C_0}{\sqrt{2}C_1}\right]^{7/11}\approx 0.5470\alpha_4^{3/8}. \tag{6.26}$$

As $\varepsilon>\varepsilon_a=\varepsilon_0'$, all modes are purely decaying. As $\alpha_4\to 0$, the null-f instability disappears, as the upper limit $\sigma'_{\max}\to 0$.

The above null-f instability was discovered by Kessler and Levine numerically (see [14]). It was later confirmed by Bensimon *et al.* in an analytical way (see [16]). Note that the quantization condition obtained by Bensimon *et al.* is in error. Nevertheless, through their quantization condition, these authors were able to draw the same conclusion as ours that the steady needle solution predicted by MSC theory was neutrally stable.

VII. THE SELECTION CONDITIONS OF DENDRITE GROWTH

In the above, we have studied the stability property of the nonclassic, steady or slightly time-dependent, needle solutions. The asymptotic results for the spectrum of complex eigenvalues have been verified by the numerical solutions in [30].

In the asymptotic analysis, we set $\overline{t}$ fixed, and let $\varepsilon\to 0$. It is found that the system of dendrite growth is controlled by the entirely new instability mechanisms, compared with the well-known Müllins-Sekerka instability. These new instability mechanisms are the GTW and null-f instability. Based on the understanding of these instability mechanisms, the selection criteria of dendrite growth at the later stage of evolution can be naturally derived. Let us consider the evolution of our basic solutions under a fixed operation condition, as $t\to\infty$. For this purpose, we define a new parameter as

$$\tilde{\varepsilon}=\sqrt{l_c U/\kappa}/\,\eta_0^2, \tag{7.1}$$

where U is the velocity of the dendrite's tip. Evidently, as $U=U$, $\tilde{\varepsilon}=\varepsilon$. For a given operation condition, α_4 is fixed; the parameter $\tilde{\varepsilon}$ associated with the growing dendrite under the investigation may vary. Hence the state point of our dynamical system, specified by $(\alpha_4,\tilde{\varepsilon})$, moves with time in the parameter plane $(\alpha_4,\tilde{\varepsilon})$. We plot the neutral curve $\{\gamma_0\}$ for the A mode $(n=0)$ of the GTW mechanism, and the neutral curve $\{\mathscr{C}_0\}$ for the S mode $(n=0)$ of the null-f mechanism in the parameter plane $(\alpha_4,\tilde{\varepsilon})$, as shown in Fig. 6. These two neutral curves intersect each other at a critical number $\alpha_c=0.1840$. This critical number will be reduced to $\alpha_c=0.1334$, provided one uses $\mathscr{K}=1.09$ in (6.24), as suggested by MSC theory. As explained before, for more accurate critical number α_c, one needs to include the higher-order approximations of the GTW and null-f mode solutions. In fact, we have computed the neutral curve $\{\gamma_0\}$ of GTW

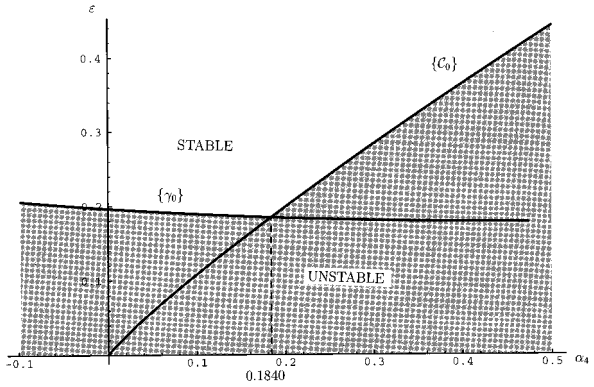

FIG. 6. The neutral curves $\{\gamma_0\}$ and $\{\mathscr{C}_0\}$, and the stability diagram of dendrite growth in the parameter plane (α_4,ε).

modes with the first-order approximation, $\sigma=\sigma_0+\varepsilon\sigma_1$. The resultant critical number α_c is then reduced to $\alpha_c=0.1153$.

The shaded region below these two curves is the unstable region, while the remaining region is a stable region. In general, given α_4 when $\tilde{t}\to\infty$, the basic solution is expected to show one of the following three types of behavior: (1) It may approach a steady solution describing a smooth growing needle; (2) it may approach a time periodic solution, describing an oscillatory growing dendrite; or (3) it may have no limit solution. The solution evolves with many short time and length scales and exhibits a chaotic pattern. On the other hand, on the basis of general linear stability theory, it can be proved that if the state point has a steady limit, this fixed point limit, in our case, must be on the the neutral curve $\{\mathscr{C}_0\}$; furthermore, if the state point approaches a time periodic orbit, this orbit must be around a point on the neutral curve $\{\gamma_0\}$. Therefore we draw the following conclusions.

(1) If the dendrite growth system exhibits a steady pattern as $t\to\infty$, as stated in the above case (1), the limiting steady solution must be on the neutral curve $\{\mathscr{C}_0\}$, and it occurs only when $\alpha_4\geqslant\alpha_c$. In other words, for the small anisotropic surface tension case, when $\alpha_4<\alpha_c$, the steady needle solution cannot be observable, due to the existence of a number of growing oscillatory GTW modes. The selection criteria given by the MSC theory are apparently not applicable in this range.

(2) If the dendrite exhibits a time periodic oscillatory pattern as $t\to\infty$, as stated in the above case (2), the limit solution must be a neutral mode on the neutral curve $\{\gamma_0\}$ and it occurs only when $0\leqslant\alpha_4\leqslant\alpha_c$. The unsteady oscillatory pattern determined by the GTW neutral mode is self-sustained. It can be stimulated by an imposed initial perturbation and does not need a continuously acting noise for its persistence. We emphasize that this statement has two implications. First, it implies that for the large anisotropic surface tension case, when $\alpha_4>\alpha_c$, no self-sustained, oscillatory dendrite is possible. In this range, one may still see a time-dependent, oscillatory structure on a steady, smooth dendrite interface induced by the decaying GTW modes. But this pattern can be sustained only by some external continuously acting forces, such as noises. Once these external forces cease, such oscillatory structure would disappear with time. Second, the criterion $(\alpha_4<\alpha_c)$ is the necessary condition for the occurrence

of a time-dependent, oscillatory dendrite growth. It has not been proved as the sufficient condition for such a linear neutrally stable mode to be attainable with any kind of initial conditions.

(3) If the dendrite growth system exhibits a chaotic pattern as $t\rightarrow\infty$, as stated in the above case (3), the state point of the system must remain in the unstable region.

The above conclusions appear to be in good agreement with experimental observations. So far most experiments for dendrite growth from a pure melt are three dimensional. These experimental results show little correlation between the selected values $\tilde{\varepsilon}=\varepsilon_*$ and the anisotropy (refer to [35]). These results, in agreement with our theory, suggest that the anisotropy for these materials is in the range of $0\leqslant\alpha_4\leqslant\alpha_c$ and the realistic dendrite growth is attracted to the neutral GTW mode, as $t\rightarrow\infty$.

Recently, several groups of researchers have performed a series of numerical simulations for the initial value problem of two-dimensional dendrite growth ([36,37]). Our results are also in good agreement with their numerical simulation results. Ihle and Müller-Krumbhaar have made numerical simulations with various values of the anisotropy. They show that as $\alpha_4=0.15$, the numerical solutions are attracted to the neutral mode of the null-f mechanism. At the later stage of evolution, the dendrite has a smooth interface with no sidebranching. Then, as $\alpha_4=0.1$, a strong time-oscillatory instability occurs; the tip radius has up to 10% fluctuation with time; as $\alpha_4=0.05$, the initially steady needle solution undergoes ''strongly irregular sidebranching and large fluctuation in tip radius and velocity.'' At the end of the computation for this case, the tip velocity is still noticeably changing and the numerical result on the tip radius $R_{\rm tip}$ and $V_{\rm tip}$ shows the inconsistency with the scaling law (6.24). These numerical simulation results apparently verify the existence of the GTW instability mechanism and suggest that the system is indeed dominated by this GTW mechanism, as α_4 is smaller than a critical number, which, from these numerical results, can be considered to be in the range $0.05<\alpha_c\leqslant0.1$. The numerical simulations conducted by Brener, Müller-Krumbhaar, Saito, and Shiraishi in terms of quasistatic approximation show the same scenario. Their results suggest $0.068<\alpha_c\leqslant0.125$.

As these numerical simulations confirm the existence of the unstable GTW modes, from here, one can logically deduce that the system must have the GTW neutral mode. This GTW neutral mode was indeed found by the numerical solutions of the eigenvalue problem (see [30]). However, so far it has not been found in the numerical simulations of the initial value problem by Ihle and Müller-Krumhbaar and others. One of the possible reasons for this may be that they did not use a proper initial condition. The steady Ivantsov solution that they used as the initial condition is apparently too far away from the GTW neutral mode solution. As indicated before, the existence of the GTW neutral mode is only a necessary condition, but not the sufficient condition attracting the solutions for the initial value problem with any kind of initial conditions, as $t\rightarrow\infty$. In general, a dynamic system that has an isolated, limit circle solution may not be attracted to this limit circle, under some initial conditions. Not only that, this limit circle might never be observed, if some nonlinear instability mechanism exists.

Therefore we have the following open questions. In order for the solutions for the initial value problem to approach the GTW neutral mode solutions as $t\rightarrow\infty$, what kind of initial conditions are required? In order for the numerical solutions for the initial value problem to approach the GTW neutral mode solutions as $t\rightarrow\infty$, what kind of algorithms are adoptable? To resolve these challenging problems, much more extensive analytical and numerical work is needed.

ACKNOWLEDGMENT

This research was supported by Operating Grants of Natural Science and Engineering Research Council of Canada (NSERC).

[1] G. P. Ivantsov, Dok. Akad. Nauk SSSR **58**, 567 (1947).
[2] G. Horvay and J. W. Cahn, Acta Metall. **9**, 695 (1961).
[3] G. E. Nash and M. E. Glicksman, Acta Metall. **22**, 1283 (1974); **22**, 1291 (1974).
[4] R. J. Schaefer, M. E. Glicksman, and J. D. Ayers, Philos. Mag. **32**, 725 (1975).
[5] M. E. Glicksman, R. J. Schaefer, and J. D. Ayers, Metall. Trans. A **7**, 1747 (1976).
[6] J. S. Langer and H. Müller-Krumbhaar, Acta Metall. **26**, 1681 (1978); **26**, 1689 (1978); **26**, 1697 (1978).
[7] J. S. Langer, Rev. Mod. Phys. **52**, 1 (1980).
[8] S. C. Huang and M. E. Glicksman, Acta Metall. **29**, 701 (1981).
[9] J. S. Langer, in *Lectures in the Theory of Pattern Formation*, USMG NATO AS Les Houches Session XLVI 1986, edited by J. Souletie, J. Vannimenus, and R. Stora (Elsevier, Amsterdam, 1987).
[10] D. A. Kessler, J. Koplik, and H. Levine, Adv. Phys. **37**, 255 (1988).
[11] M. Kruskal and H. Segur, Stud. Appl. Math. **85**, 129 (1991).
[12] J. M. Hammersley and G. Mazzarino, IMA J. Appl. Math. **42**, 43 (1989).
[13] *Asymptotics Beyond All Orders*, Vol. 284 of *NATO Advanced Study Institute, Series B: Physics*, edited by H. Segur, S. Tanveer, and H. Levine (Plenum, New York, 1991).
[14] D. A. Kessler and H. Levine, Phys. Rev. Lett. **57**, 3069 (1986).
[15] P. Pelce and Y. Pomeau, Stud. Appl. Math. **74**, 245 (1986).
[16] D. Bensimon, P. Pelce, and B. I. Shraiman, J. Phys. (Paris) **48**, 2081 (1987).
[17] M. N. Barber, A. Barbieri, and J. S. Langer, Phys. Rev. A **36**, 3340 (1987); J. S. Langer, *ibid.* **36**, 3350 (1987).
[18] J. J. Xu, in *Structure and Dynamics of Partially Solidified System*, Vol. 125 of *NATO Advanced Study Institute, Series E*, edited by D. E. Loper (Plenum, New York, 1987), p. 97.

[19] A. Dougherty and J. P. Gollub, Phys. Rev. A **38**, 3043 (1988).
[20] D. Kessler, J. Koplik, and H. Levine, Adv. Phys. **37**, 255 (1988).
[21] P. Pelce, *Dynamics of Curved Front* (Academic, New York, 1988).
[22] J. J. Xu, Phys. Rev. A **37**, 3087 (1988).
[23] J. J. Xu, J. Cryst. Growth **100**, 481 (1990).
[24] J. J. Xu, Stud. Appl. Math. **82**, 71 (1990).
[25] J. J. Xu, Phys. Rev. A **43**, 930 (1991).
[26] J. J. Xu, Physics (D) **51**, 579 (1991).
[27] J. J. Xu and Z. X. Pan, J. Cryst. Growth **129**, 666 (1993).
[28] J. J. Xu, J. Fluid Mech. **263**, 227 (1994).
[29] J. J. Xu, Can. J. Phys. **72**, 120 (1994).
[30] J. J. Xu and Z. X. Pan, McGill University, ISSN 0824-4944, Report No. 93-05, 1993 (unpublished).
[31] J. J. Xu, McGill University, ISSN 0824-4944, Report No. 94-10, 1994 (unpublished).
[32] E. A. Brener and V. I. Melnikov, Adv. Phys. **40**, 53 (1991).
[33] J. S. Langer, Phys. Today **10**, 24 (1992).
[34] M. Ben Amar and E. A. Brener, Phys. Rev. E **47**, 534 (1993).
[35] M. E. Glicksman and S. P. Marsh, in *Handbook of Crystal Growth*, edited by D. T. J. Hurle (Elsevier, Amsterdam, 1993), Vol. 1, Chap. 15.
[36] T. Ihle and H. Müller-Krumbhaar, Phys. Rev. E **49**, 2972 (1994).
[37] E. Brener, T. Ihle, H. Müller-Krumbhaar, Y. Saito, and K. Shiraishi, Physica A **204**, 96 (1994).